






## RESEARCH ARTICLE

# PANI/Zn-Cu ferrite polymer composites as free-standing high dielectric materials

Tamilarasi Kumar<sup>1</sup>  | Aji Udhaya Paul Raj<sup>2</sup>  | Meena Muthukrishnan<sup>1</sup>  |  
Senthil Muthu Kumar Thiagamani<sup>3,4,5</sup>  | Mohamed Hashem<sup>6</sup> |  
Shaikh Ayaz Mukarram<sup>7</sup> 

<sup>1</sup>Department of Physics, S.T. Hindu College (Affiliated to Manonmaniam Sundaranar University, Abishekapatti, Tirunelveli-627012), Nagercoil, Tamil Nadu, India

<sup>2</sup>Department of Physics, Holy Cross College, Nagercoil, Tamil Nadu, India

<sup>3</sup>Department of Mechanical Engineering, Kalasalingam Academy of Research and Education, Krishnankoil, Tamil Nadu, India

<sup>4</sup>Department of Mechanical Engineering, INTI International University, Nilai, Negeri Sembilan, Malaysia

<sup>5</sup>Centre for Advanced Composite Materials (CACM), Universiti Teknologi Malaysia, Johor Bahru, Malaysia

<sup>6</sup>Department of Dental Health, College of Applied Medical Sciences, King Saud University, Riyadh, Saudi Arabia

<sup>7</sup>Institute of Food Science, University of Debrecen, Hungary

## Correspondence

Meena Muthukrishnan, Department of Physics, S.T. Hindu College (Affiliated to Manonmaniam Sundaranar University, Abishekapatti, Tirunelveli-627012), Nagercoil 629002, Tamil Nadu, India. Email: [meenaraj19@gmail.com](mailto:meenaraj19@gmail.com)

Senthil Muthu Kumar Thiagamani, Department of Mechanical Engineering, Kalasalingam Academy of Research and Education, Anand Nagar, Krishnankoil 626126, Tamil Nadu, India. Email: [tsmkumar@klu.ac.in](mailto:tsmkumar@klu.ac.in)

## Funding information

King Saud University, Grant/Award Number: RSPD2024R680

## Abstract

In a wide range of applications, from consumer electronics to cutting-edge industrial and scientific equipment, high dielectric permittivity ( $\epsilon'$ ) polymers are crucial for maximizing the performance and efficiency of electrical and electronic systems. Researchers strive to create and perfect these materials to meet the changing demands of modern technology. It is generally known that freestanding bare polymers cannot achieve high dielectric values; however, the mixing of multiple materials that are distinct is an effective technique for developing high dielectric hybrids. Polymer-based nanoarchitectures are particularly beneficial for use in the storage of energy due to characteristics such as excellent mechanical strength, noncorrosive nature, lightweight, affordability, versatility, thermal and electrical shielding. The primary aim of this investigation is to prepare copper ferrite, zinc ferrite, and copper<sub>0.5</sub>zinc<sub>0.5</sub> ferrite (CuFe<sub>2</sub>O<sub>4</sub>, ZnFe<sub>2</sub>O<sub>4</sub>, and Cu<sub>0.5</sub>Zn<sub>0.5</sub>Fe<sub>2</sub>O<sub>4</sub>) nanoparticle (NP) via combustion technique using egg albumen as a fuel and these NPs were separately dispersed in polyaniline (PANI) matrix by the method of ex situ polymerization of aniline with an objective to enhance the electrical properties for energy storage and electromagnetic wave applications. Flexible freestanding films were casted via solution casting technique. X-ray diffractogram of 5 wt.% NP dispersed PANI films confirmed the presence of NPs in the PANI matrix. Scanning electron micrograph images show the homogeneous dispersion of NPs into PANI matrix. Rather than the pure ferrite NPs, mixed ferrite highly enhance the permittivity of PANI films without much increasing its loss factor, the obtained values of  $\epsilon'$  of all the three ferrite added films are higher than polyvinylidene fluoride (PVDF)/(Mn<sub>0.2</sub>Zr<sub>0.2</sub>Cu<sub>0.2</sub>Ca<sub>0.2</sub>Ni<sub>0.2</sub>)Fe<sub>2</sub>O<sub>4</sub> nanofiller. In this work notably for 5 wt.% Cu<sub>0.5</sub>Zn<sub>0.5</sub>Fe<sub>2</sub>O<sub>4</sub> dispersed film shows the highest value of  $\epsilon'$  (7291) for 100 Hz at 150°C with ultralow loss factor (0.08) which is the key characteristic of an energy storage material. Thus, this present study leads the formation of a cost effective, flexible, high dielectric material, which can be a potential alternate to replace PVDF/(Mn<sub>0.2</sub>Zr<sub>0.2</sub>Cu<sub>0.2</sub>Ca<sub>0.2</sub>Ni<sub>0.2</sub>)Fe<sub>2</sub>O<sub>4</sub> and polyvinyl alcohol/Ni<sub>0.65</sub>Cu<sub>0.35</sub>Fe<sub>2</sub>O<sub>4</sub> polymer blends for energy storage applications.

## KEYWORDS

dielectric properties, nanoparticles, PANI, polymer composites

## 1 | INTRODUCTION

Because of technological developments, there is a growing interest in microelectronics, particularly capacitors in integrated circuits, which ultimately call for a dielectric material with a reasonably high dielectric constant.<sup>1–5</sup> Compact and sustainable power systems need dielectric materials with high energy density, low dielectric loss, and high efficiency.<sup>6,7</sup> The performance of dielectric materials determines a great deal of capacitor performance and the development of high energy densities and low dielectric loss. In general, polymer dielectrics have been regarded as the best option for many power applications, including electrochemical capacitors, power conditioning, and numerous power electronics.<sup>8,9</sup> However, the comparatively low energy density continues to be a significant issue and restricts the continued use of polymer-based capacitors. High-dielectric constant inorganic nanoparticles are most commonly used with organic polymers to create polymer nanocomposite dielectrics with high energy densities. Flexible polymer nanocomposite dielectric materials are one of the potential polymer dielectrics for energy storage applications.

Many researchers have reported on the synthesis and characterization of high dielectric materials. Using the coprecipitation process, Kakade et al.<sup>10</sup> prepared the multiferroic composite  $x[\text{Co}_{0.9}\text{Ni}_{0.1}\text{Fe}_2\text{O}_4] - (1-x)[0.5\text{Ba}_{0.7}\text{Ca}_{0.3}\text{TiO}_3 - 0.5\text{BaZr}_{0.2}\text{Ti}_{0.8}\text{O}_3]$ . The fabricated composites were subjected to dielectric testing, relaxation spectrum, modulus, magnetodielectric properties, X-ray diffraction (XRD), and scanning electron micrograph (SEM). A high dielectric constant and loss factor were obtained for the value of  $x = 0.5$  in the  $x[\text{Co}_{0.9}\text{Ni}_{0.1}\text{Fe}_2\text{O}_4] - (1-x)[0.5\text{Ba}_{0.7}\text{Ca}_{0.3}\text{TiO}_3 - 0.5\text{BaZr}_{0.2}\text{Ti}_{0.8}\text{O}_3]$  composite. The high loss factor of 3.3 and a high dielectric constant that is almost equal to 11,000 were also recorded in their study.

Polyaniline (PANI) is one of the polymeric dielectric materials that come in a range of shapes with various chemical and physical characteristics.<sup>11,12</sup> Its simplicity in preparation, light weight, low cost, better suspension ability, low dimensional systems, relatively large surface area, better electrical, and optical characteristics, extremely stable in air and soluble in a variety of solvents, and excellent processibility are all advantages.<sup>13,14</sup> When compared with pure PANI film, inorganic dispersed organic polymer films exhibit improved processing capabilities and anticorrosion characteristics in addition to enhanced dielectric properties. The main advantage of inorganic filling is that it is nontoxic. Out of all inorganic fillers, ferrite fillers are more crucial due to their stable crystal structure, good magnetic properties, high electrical properties, and the spinel ferrites are widely used in electronic devices, magnetic materials based on them have attracted a lot of attention.<sup>15–19</sup> Because of low-dimensional electrical system applications, nanoscopic sized filler particles are in polymer matrix, such a combination exhibits improved electrical characteristics. Because of their spinel structure, ferrites are a prominent filler material used by scientists for improving the electrical features of pure polymers.<sup>20</sup> It has been proven that ferrite nanoparticles (NPs) may be used as nanocatalysts for biodiesel production, tunable phase shifters, and anisotropy in soft magnetic applications.<sup>21–23</sup>

Numerous studies on the creation, characterization, and properties of polymer-ferrite NP are described in the literature.<sup>24,25</sup> PANI is

one of the most useful conducting polymers, because of its high absorption coefficients in visible light, intriguing redox properties, less density than metallic substances, energy storage, ease of synthesis, relatively excellent conductivity, ecologically stable compound, cheapness, beneficial optical and electrical characteristics, and ability to be reversibly converted from conduction to insulation through the use of acid–base reactions or electrochemical or chemical doping.<sup>26–29</sup> Conducting polymer PANI with different nanocomposites shows different application fields such as waste water treatment, biomedical applications, and electromagnetic wave absorptions.<sup>30–33</sup>

The use of PANI-Zn-Cu ferrite materials is justified by their special set of qualities, which enable them to be used in a wide range of applications. Ferrites are magnetic materials usually made of iron oxide compounds, while PANI is a conducting polymer. When PANI and ferrites are combined, a composite material is created with improved beneficial properties. The main advantages and reasons for using PANI-Zn-Cu ferrite materials are its conductivity, magnetic and tunable characteristics, sensitivity to external stimuli, biocompatibility, and multifunctionality.<sup>34,35</sup> However, there are a few challenges in using PANI-Zn-Cu ferrite materials. The synthesis is a complicate process with several steps, and one of the main challenges is getting a uniform distribution in the PANI matrix. Additional negatives include potential effects on mechanical properties and cost effectiveness resulting from the high cost of raw materials. Complete characterization and fine-tuning are essential for optimizing the realistic applicability of these composites.

Few researchers have investigated PANI/ferrites, and further research is still needed.<sup>36–38</sup> PANI-Zn<sub>0.2</sub>Mn<sub>0.8</sub>Fe<sub>2</sub>O<sub>4</sub> ferrite core-shell composite was synthesized by Khairy et al.<sup>36</sup> using in situ chemical oxidation polymerization. These composite samples were characterized by XRD, Fourier transform infrared (FTIR), transmission electron microscopy (TEM), thermogravimetric analysis, vibrating sample magnetometer, and dielectric measurements. In their research, pure PANI exhibited real part of dielectric constant nearly 3800 and imaginary part of dielectric constant nearly 10,000. Chitra et al.<sup>37</sup> prepared PANI/Ni<sub>(1-x)</sub>Co<sub>x</sub>Fe<sub>2</sub>O<sub>4</sub> nanocomposite via an in situ chemical oxidative polymerization. The FTIR, UV–visible spectra, dielectrics, and XRD were used to characterize the nanocomposites. The 10% and 20% w/w prepared PANI/Ni<sub>(1-x)</sub>Co<sub>x</sub>Fe<sub>2</sub>O<sub>4</sub> nanocomposites showed high dielectric constant approximately 17,000 and 200 at 100°C for 100 Hz whereas the corresponding loss factor was found to be nearly 7 and 8, respectively.

PANI and Co<sub>0.6</sub>Zn<sub>0.4</sub>Fe<sub>2</sub>O<sub>4</sub> NPs were synthesized using in situ polymerization process by Gabal et al.<sup>38</sup> They were characterized by alternating conductivity (AC)-conductivity, dielectric measurements, XRD, FT-IR, and TEM measurements. The frequency dependence of the real dielectric constant ( $\epsilon'$ ) and imaginary dielectric constant ( $\epsilon''$ ) of the prepared samples have high value as  $10^6$  and  $10^7$ , respectively. PANI ferrite composites have exceptional dielectric capabilities, but their significant dielectric loss makes them unsuitable for employment in emerging technologies. It is required to develop flexible films with high dielectric strength, low loss factor, and higher thermal stability in order to envision potential advances in power systems and energy

storage devices. In this context, the authors aimed to prepare PANI polymer films using inexpensively prepared ferrites as filler.

In this article, for the first time 5 wt.% of  $\text{CuFe}_2\text{O}_4$ ,  $\text{ZnFe}_2\text{O}_4$ , and  $\text{Cu}_{0.5}\text{Zn}_{0.5}\text{Fe}_2\text{O}_4$  NPs synthesized via green method was dispersed in PANI films. The prepared NP's performance in our previous research<sup>39</sup> having been pointed out, it showed that the narrow particle size and morphology obtained in our present study could help to tune the properties of PANI films. As a result, the  $\text{CuFe}_2\text{O}_4$ ,  $\text{ZnFe}_2\text{O}_4$ , and  $\text{Cu}_{0.5}\text{Zn}_{0.5}\text{Fe}_2\text{O}_4$  nanoferrites will be utilized in the present investigation to create PANI polymer nanocomposites.

According to the literature there are many biopolymers and bio-products doped polymer composites for various applications.<sup>40–43</sup> In accordance to that, in the current research through an eco-friendly procedure the ferrite NPs were synthesized using egg albumen as fuel. The novelty of this work lies in the green synthesized ferrite NPs dispersed in conducting PANI by ex situ polymerization to enhance the electrical behavior of bare PANI films. In order to research and analyze the impact of ferrite filler on the structural, morphological, and electrical characteristics in PANI matrix, 5 wt.% of  $\text{CuFe}_2\text{O}_4$ ,  $\text{ZnFe}_2\text{O}_4$ , and  $\text{Cu}_{0.5}\text{Zn}_{0.5}\text{Fe}_2\text{O}_4$  NP was dispersed in PANI matrix. To the best of our knowledge, no such extensive study with the use of copper–zinc ferrites produced using this novel egg albumen fuel solution-combustion route dispersed PANI films has been published in literature.

## 2 | MATERIALS AND METHODS

### 2.1 | Materials

Ferric nitrate nonahydrate  $\text{Fe}(\text{NO}_3)_3 \cdot 9\text{H}_2\text{O}$ , cupric nitrate hexahydrate  $\text{Cu}(\text{NO}_3)_2 \cdot 6\text{H}_2\text{O}$ , zinc nitrate hexahydrate  $\text{Zn}(\text{NO}_3)_2 \cdot 6\text{H}_2\text{O}$ , 35% dilute HCl, aniline hydrochloride  $\text{C}_6\text{H}_5\text{NH}_2\text{HCl}$ , and potassium dichromate  $\text{K}_2\text{Cr}_2\text{O}_7$  were purchased from Aldrich and were used as precursor without further purification. Freshly prepared egg white solution was used as a solvent for the synthesis of NPs.

### 2.2 | Fabrication of nanocomposites

$\text{CuFe}_2\text{O}_4$ ,  $\text{ZnFe}_2\text{O}_4$ , and  $\text{Cu}_{0.5}\text{Zn}_{0.5}\text{Fe}_2\text{O}_4$  NPs were prepared by solution combustion method using egg albumen as fuel. The precursors, such as  $\text{Fe}(\text{NO}_3)_3 \cdot 9\text{H}_2\text{O}$ ,  $\text{Cu}(\text{NO}_3)_2 \cdot 6\text{H}_2\text{O}$ , and  $\text{Zn}(\text{NO}_3)_2 \cdot 6\text{H}_2\text{O}$  were added gradually to the egg white solution in a stoichiometric molar ratio. The mixture was then constantly stirred for about 2 h without any pH modification. At last, the mixture was allowed to dry at  $80^\circ\text{C}$ , revealing the dark brown ash powder, which was later annealed at  $600^\circ\text{C}$  for 2 h. The 5 wt.% of  $\text{CuFe}_2\text{O}_4$ ,  $\text{ZnFe}_2\text{O}_4$ , and  $\text{Cu}_{0.5}\text{Zn}_{0.5}\text{Fe}_2\text{O}_4$  dispersed PANI films were casted by simple solution casting technique. The polymerization of aniline with an oxidative agent such as ammonium persulfate (APS) has been the common method reported for PANI production.<sup>44,45</sup> In this work, the APS was replaced by potassium dichromate due to safety considerations and to reduce

toxicity. Potassium dichromate has the advantages of requiring less time for the polymerization of aniline molecules and producing a greater yield percentage of PANI. While employing APS, the polymerization reaction requires a lower refrigeration temperature for approximately 10–12 h to complete. However, using potassium dichromate, no further cooling temperature is necessary for polymerization. In this work, 0.1 M (12.96 g) of aniline hydrochloride with 1.0 N HCl solution of deionized water was added drop by drop with the oxidizing agent of 0.025 M (7.36 g) potassium dichromate with 1.5 N HCl solution. These solutions were mixed thoroughly for about 2 h in a constant temperature ( $80^\circ\text{C}$ ) bath leading to the formation of dark green colored PANI solution. Later by using a Buchner funnel the solution was filtered and final product in powder form was obtained. The obtained powder was then washed several times using deionized water and dried at  $80^\circ\text{C}$  for 24 h. The powder was dissolved in a very low concentrated aqueous polyvinyl alcohol (nearly 1 PPM) solution and casted into film by pouring into a petri dish. Finally, the casted films of 9 cm diameter were dried and peeled off and cut in to several pieces for further characterization. The calculated amount of 5 wt.% of prepared  $\text{CuFe}_2\text{O}_4$ ,  $\text{ZnFe}_2\text{O}_4$ , and  $\text{Cu}_{0.5}\text{Zn}_{0.5}\text{Fe}_2\text{O}_4$  via combustion technique using egg albumen were dispersed separately under final stage of stirring for the preparation of  $\text{CuFe}_2\text{O}_4$ ,  $\text{ZnFe}_2\text{O}_4$ , and  $\text{Cu}_{0.5}\text{Zn}_{0.5}\text{Fe}_2\text{O}_4$  dispersed PANI films.

### 2.3 | Characterization

Before dispersion, the as prepared ferrites particles were subjected to XRD analysis using a Shimadzu XRD7000 X-ray diffractometer in the scanning rate of 40 kV/30 mA for the  $2\theta$  range  $10^\circ$ – $80^\circ$ . The FTIR spectra of PANI was recorded using a Perkin Elmer spectrometer within the wavenumber range of  $4000$ – $500\text{ cm}^{-1}$ . The morphology of the synthesized NPs was recorded using a Carl Zeiss Gemini 300 FESEM instrument. The dielectric measurements were carried out in the temperature range of  $40$ – $150^\circ\text{C}$  and frequency range of  $100$ – $1\text{ MHz}$ , using LCR meter (AGILENT 4284A) with an accuracy of  $\pm 2\%$ .

## 3 | RESULTS AND DISCUSSIONS

### 3.1 | XRD analysis

The XRD pattern of ferrites particles is depicted in Figure 1A. It is evident that, the prepared fillers were crystallized in cubic structure.<sup>46–48</sup> Figure 1B illustrates the XRD patterns of pure PANI and 5 wt.% NPs dispersed PANI films. The prominent diffraction peaks at  $15.01^\circ$ ,  $20.81^\circ$ , and  $25.51^\circ$  can be seen in bare PANI, which were very well matched the published results.<sup>49,50</sup> Using Debye Scherrer's formula,<sup>51</sup> the average crystallite size of the filler before dispersion was 42.2, 56.5, and 16.1 nm for  $\text{CuFe}_2\text{O}_4$ ,  $\text{ZnFe}_2\text{O}_4$ , and  $\text{Cu}_{0.5}\text{Zn}_{0.5}\text{Fe}_2\text{O}_4$ , which was lower than reported by any other method, which could be due to egg albumen, whose role was explained in the previous work.<sup>39</sup>

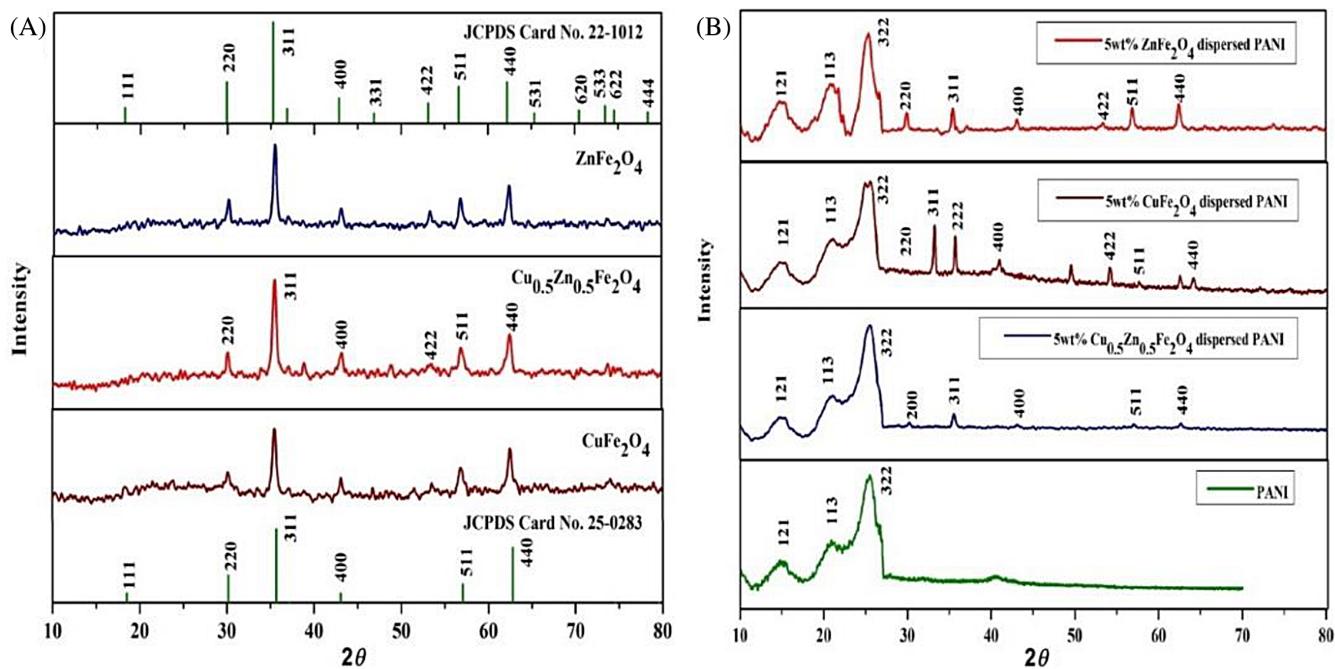


**FIGURE 1** X-ray diffraction pattern of (A) as prepared ferrites (B) pure and 5 wt.%  $\text{CuFe}_2\text{O}_4$ ,  $\text{ZnFe}_2\text{O}_4$ , and  $\text{Cu}_{0.5}\text{Zn}_{0.5}\text{Fe}_2\text{O}_4$  dispersed polyaniline (PANI) films.

Findings	5 wt.% $\text{ZnFe}_2\text{O}_4$	5 wt.% $\text{CuFe}_2\text{O}_4$	5 wt.% $\text{Cu}_{0.5}\text{Zn}_{0.5}\text{Fe}_2\text{O}_4$
$D$ (nm)	46.3	35.9	22.7
SSA ( $\text{m}^2/\text{g}$ )	108	338	423

**TABLE 1** Crystallite size of filler particles and SSA of the prepared PANI films.

Abbreviations: PANI, polyaniline; SSA, specific surface area.

By comparing Figure 1A and Figure 1B, the infusion of the NPs in the polymer matrix is evident from the appearance of new peaks in the polymer composite films, corresponding to lattice planes (311), (400), (511), and (400) of various fillers used respectively. The rise of the unique diffraction peaks associated with the well-crystalline ferrites suggested the successive incorporation of NPs in to PANI matrix. In addition, 5 wt.% of filler incorporation increases nanocrystalline phase of polymer matrix, which is an added advantage of the prepared films because nanocrystalline phases have a remarkably high absorption of organic guest molecules and have a density that is lower than that of the comparable amorphous phases, which suggest the use of these films for sensor applications.

The crystallite size of the filler NPs and the specific surface area (SSA)<sup>52–54</sup> of the prepared films obtained from XRD are displayed in Table 1.

From these findings we clearly understand that the 5 wt.%  $\text{Cu}_{0.5}\text{Zn}_{0.5}\text{Fe}_2\text{O}_4$  dispersed film shows the high SSA than the other two ferrite dispersed films. Increase in surface area increases the conductivity of the sample, this suggests that the high SSA film has more ion charge carriers to conduct electricity. The increase in effective surface area of the films linearly increases the sensitivity of the sensor when the films are used as gas sensors.<sup>55</sup> The interaction between the gas molecules and the film surfaces modifies the quantity of

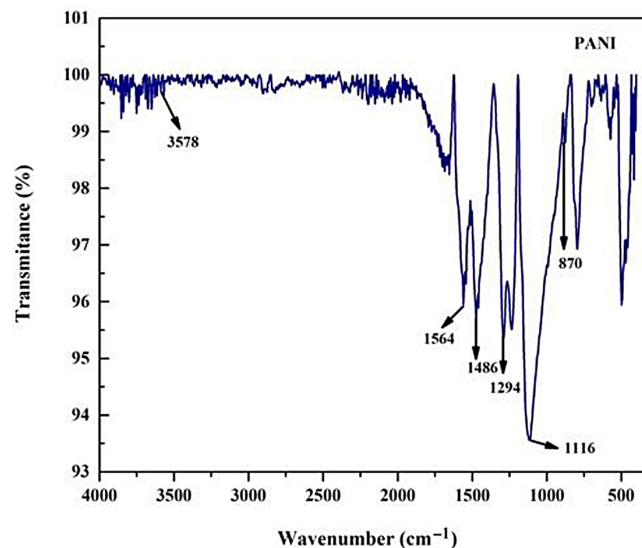


**FIGURE 2** Fourier transform infrared spectrum of pure polyaniline (PANI) film.

charge carriers and, in turn, alterations in the electrical conductivity. A more responsive and sensitive gas sensor is created by optimizing the surface area as it increases the uniformity and effectiveness of gas

adsorption, according to the linear connection between sensitivity and effective surface area.<sup>56</sup> So, achieving this type of high-effective surface area films can be suitable for gas sensor, chemical sensor, and molecular sensor applications.<sup>57,58</sup>

### 3.2 | FTIR analysis

The pure PANI FTIR spectra in Figure 2 were obtained within the wavenumber range of 4000–500  $\text{cm}^{-1}$  using Perkin Elmer spectrometer. Furthermore, the FTIR spectrum of PANI exhibits its own unique peaks at 3578, 1564, 1486, 1294, 1116, and 870  $\text{cm}^{-1}$ . The N–H stretching vibration of the secondary amine is shown by the peak at 3578  $\text{cm}^{-1}$ . The stretching vibrations of the quinoid rings N=Q=N (in which Q is the quinoid ring) and the benzenoid rings (C=C stretching vibration) are denoted by the peaks at 1564 and 1486  $\text{cm}^{-1}$ . The C–N stretching of the secondary aromatic ring is reflected by the peak at 1294  $\text{cm}^{-1}$ . The aromatic C–H in the plane of the 1,4-substituted benzenoid ring is implied by the peak at 1116  $\text{cm}^{-1}$ , and the aromatic C–H out of the plane bending vibration is represented by the peak at 870  $\text{cm}^{-1}$ . These positions of the peaks are in good agreement with the results observed in previous research.<sup>59,60</sup> These extremely powerful bands known as the quinoid and benzenoid rings were utilized to calculate the degree of oxidation (R), which is calculated as the ratio between the intensities of the bands linked to the benzenoid and quinoid rings.<sup>61</sup> This variation has to do with the oxidation of benzenoid rings, which change into quinoid rings. It also has to do with the conversion of amino groups into imino groups when the polymer oxidizes.<sup>62</sup> PANI's relative intensity ratio, as determined, is 1.00. It is evident from the obtained relative intensity ratio of 1.00 that the experiment concludes with a dark green color, which confirms that the PANI has formed in its doped emeraldine oxidation state.<sup>59</sup>

### 3.3 | Morphology analysis

Figures 3A,B, 4A,B, and 5A,B exhibited the synthesized  $\text{CuFe}_2\text{O}_4$ ,  $\text{ZnFe}_2\text{O}_4$ , and  $\text{Cu}_{0.5}\text{Zn}_{0.5}\text{Fe}_2\text{O}_4$  NPs SEM, histogram, and energy-dispersive x-ray analysis (EDAX) spectra, respectively. Carl Zeiss Gemini 300 FESEM instrument is used to record these SEM micrographs. Clear grain boundaries have been confirmed by SEM micrographs. The histogram clearly shows the homogeneous particle creation. Oxygen vacancies may be the reason for the lower percentage of oxygen in the prepared particle as revealed by EDAX, which also reveals the particle's purity.

Figure 6 shows the SEM micrographs of pure PANI,  $\text{CuFe}_2\text{O}_4$ ,  $\text{ZnFe}_2\text{O}_4$ , and  $\text{Cu}_{0.5}\text{Zn}_{0.5}\text{Fe}_2\text{O}_4$  (5 wt.%) dispersed forms of PANI films. Figure 6A illustrates the consistently linked fibrillar and extremely porous morphology of pure PANI films.

The formation of PANIs under various circumstances has previously led to the development of such fibrillar shape.<sup>51,63,64</sup> These polymers that exhibited unintended behaviors like hydrolysis, chain scission, and/or crosslinking were given this fibrillar-like shape. It is amazing to learn that prepared ferrite NP loading has a significant impact on the PANI film's morphology, and that a change in PANI morphology is seen. In addition to the presence of porosity that developed from the polymer blend matrix, it is observed that the agglomeration improved in 5 wt.%  $\text{Cu}_{0.5}\text{Zn}_{0.5}\text{Fe}_2\text{O}_4$  NP dispersed film, which signifies the superior interfacial interaction between that filler and the polymer matrices. The prepared PANI films filled with highest loading of 5 wt.% copper ferrite, zinc ferrite and copper-zinc ferrite NPs loading, the particles are tightly packed and no bare NPs are observed which indicating the potential of this method to create well dispersed films with uniformly dispersed layer.

When airborne moisture came into contact with the polymer solution's surface, it condensed to create water droplets. The outermost layer of the films that are formed can therefore grow porous.

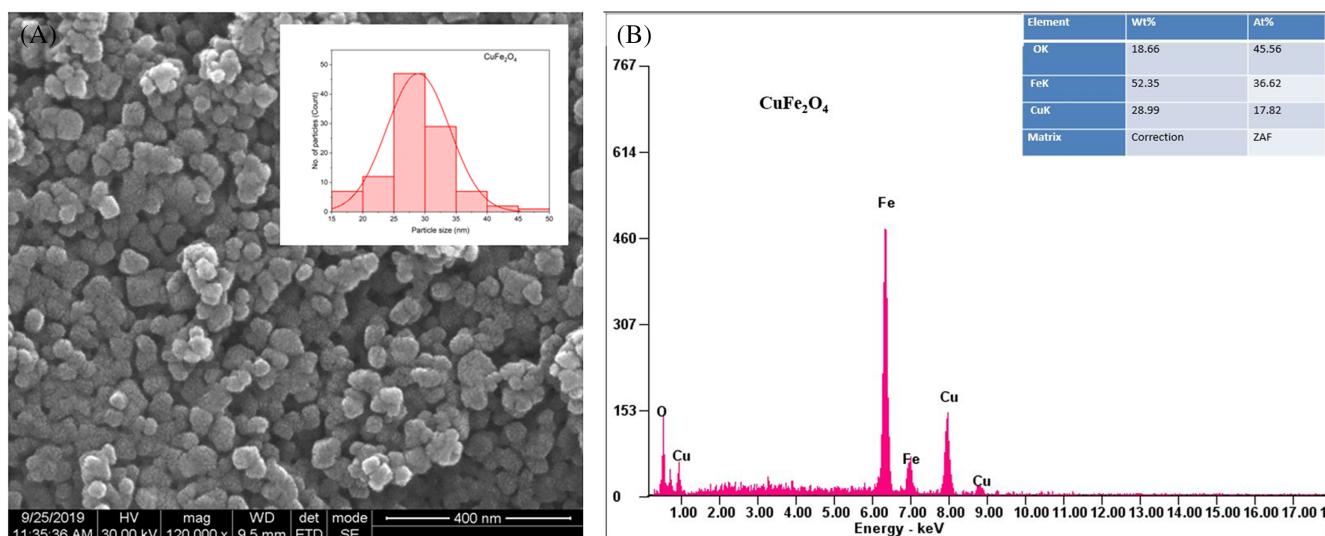


**FIGURE 3**  $\text{CuFe}_2\text{O}_4$  nano particles (A) scanning electron micrograph image with histogram and (B) energy-dispersive x-ray analysis (EDAX) spectrum.

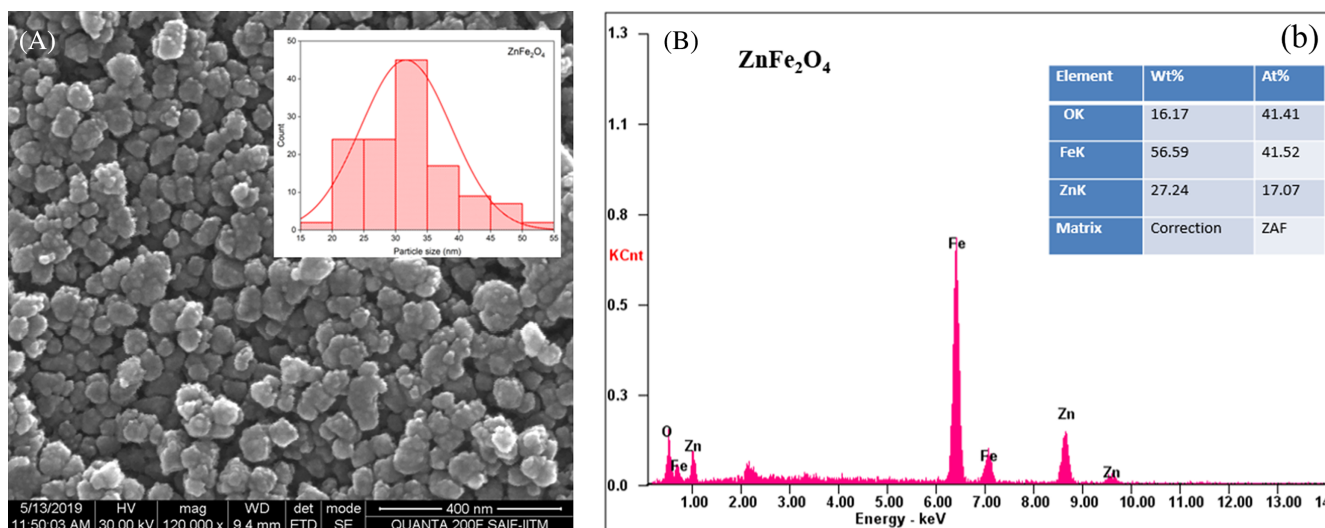


**FIGURE 4** ZnFe<sub>2</sub>O<sub>4</sub> nano particles (A) scanning electron micrograph image with histogram and (B) energy-dispersive x-ray analysis (EDAX) spectrum.

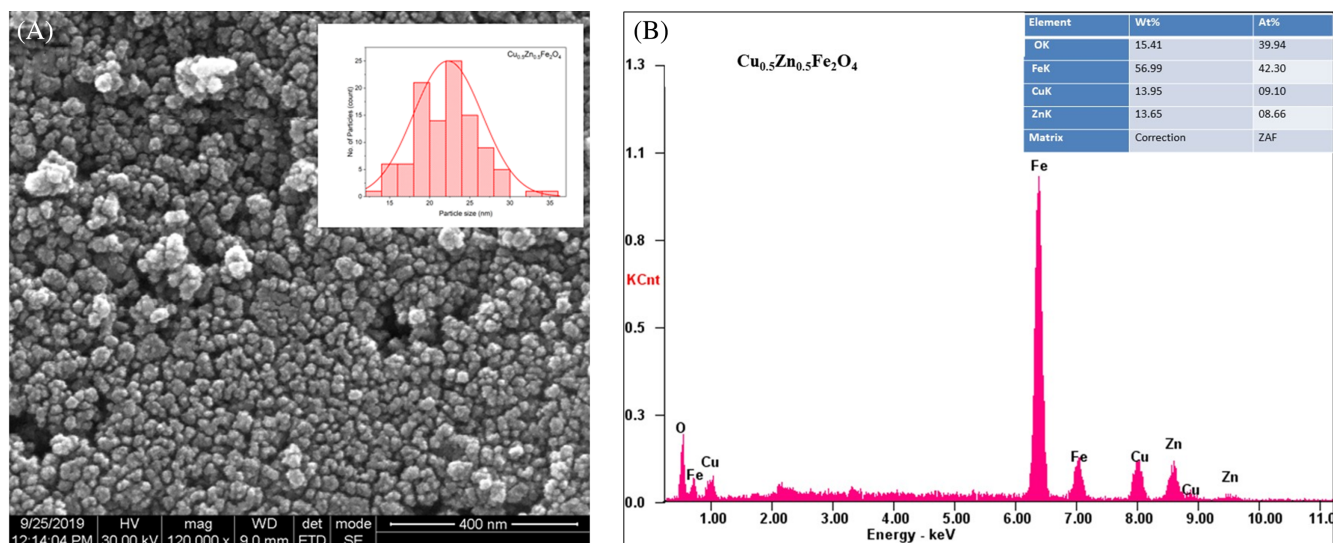


**FIGURE 5** Cu<sub>0.5</sub>Zn<sub>0.5</sub>Fe<sub>2</sub>O<sub>4</sub> nano particles (A) scanning electron micrograph image with histogram and (B) energy-dispersive x-ray analysis (EDAX) spectrum.

These pores have a negative impact on the films' conductivity and flexibility.<sup>65</sup> The image shows that using fine nanosize particles may reduce surface porosity in certain regions and increase the rate of material movements. The size controlled 5 wt.% Cu<sub>0.5</sub>Zn<sub>0.5</sub>Fe<sub>2</sub>O<sub>4</sub> NP exhibits the formation of quantity films with reduced porosity of the polymer matrix.

The porosity decreases (Table 2) at a 5 wt.% concentration of prepared NPs, and ferrite NPs act as a pore-reducing agent in this instance. It was thought that the addition of filler material affected the morphology of PANI films that were prepared. Surface roughness and electrical conductivity, however, significantly increase when porosity decreases. This is so because the electrical conductivity is mainly caused by electron conduction. Increased surface roughness is a result of inhomogeneous powder spreading and dispersing.

### 3.4 | Dielectric analysis

The measurement of complex permittivity as a function of frequency is recognized as dielectric spectroscopy. Because permanent and induced dipoles, together with ion or electron conduction, all contribute to a material's dielectric response, this analysis may additionally be performed as a function of temperature or time at fixed frequencies to determine various physical and chemical properties of a given polymer. Dielectric spectroscopy can be used to investigate polymer molecular relaxation events such as the glass transition or phase transitions. For dielectric measurements, casted films were cut into circular films with radius 6.5 mm were used. In order to make the films an effective conductive layer at room temperature, the two

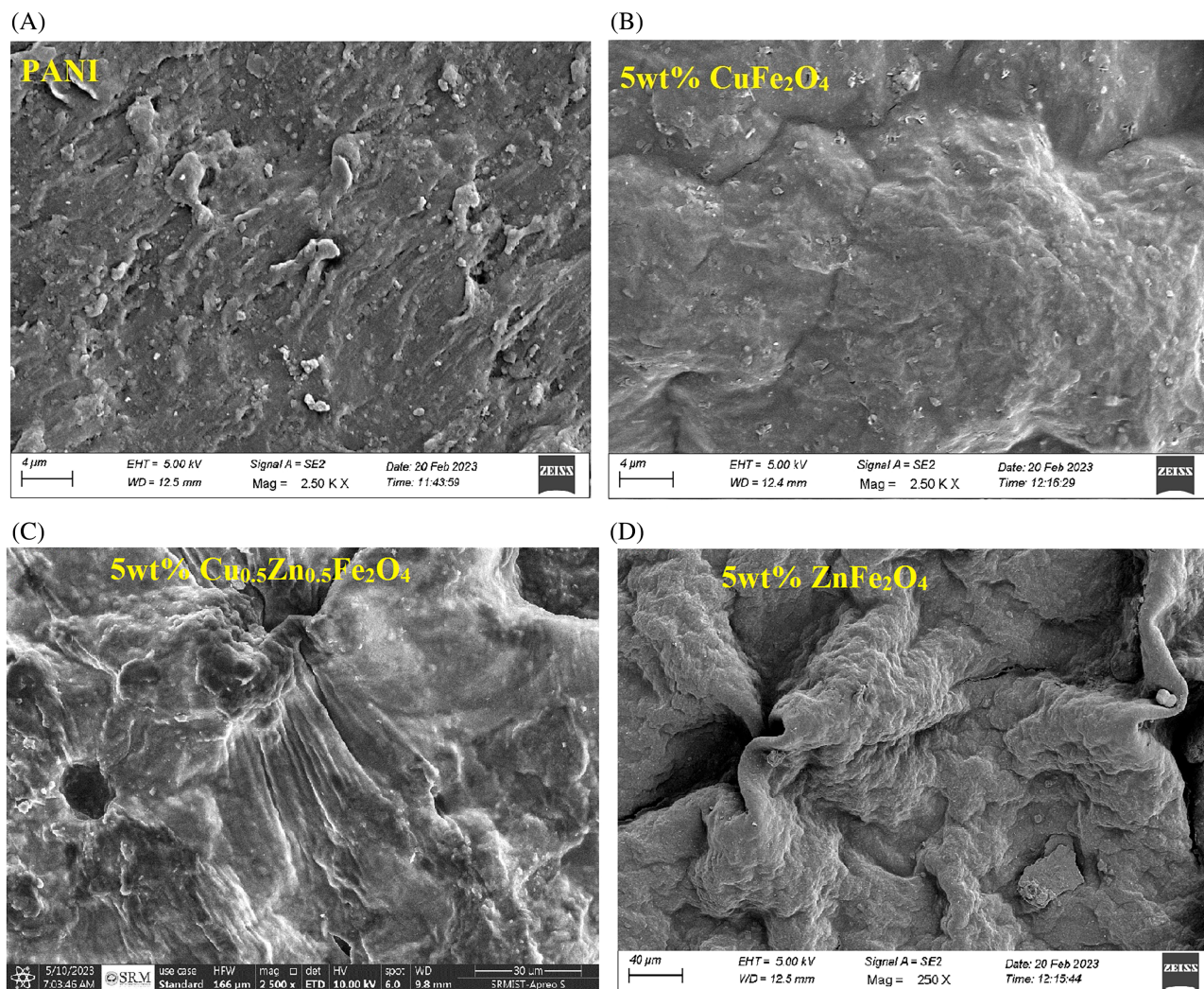


**FIGURE 6** Scanning electron micrograph analysis (A) pure polyaniline (PANI), (B) 5 wt.%  $\text{CuFe}_2\text{O}_4$ , (C)  $\text{Cu}_{0.5}\text{Zn}_{0.5}\text{Fe}_2\text{O}_4$ , and (D) 5 wt.%  $\text{ZnFe}_2\text{O}_4$  dispersed PANI films.

**TABLE 2** Porosity of 5 wt.% of as prepared NP's dispersed PANI films.

Sample name	Porosity (%)
PANI film	9.91
5 wt.% $\text{CuFe}_2\text{O}_4$ embedded PANI film	1.01
5 wt.% $\text{ZnFe}_2\text{O}_4$ embedded PANI film	1.89
5 wt.% $\text{Cu}_{0.5}\text{Zn}_{0.5}\text{Fe}_2\text{O}_4$ embedded PANI film	0.64

Abbreviations: NP, nanoparticle; PANI, polyaniline.

opposing sides of the films were painted with silver.<sup>66</sup> The sample was positioned between two metal electrodes during the two-probe setup's AC conductivity measurements.<sup>67</sup> The dielectric measurements were carried out in the temperature range of 40–150°C and frequency range of 100–1 MHz, using LCR meter (AGILENT 4284A) with an accuracy of  $\pm 2\%$ .<sup>68,69</sup> The real ( $\epsilon'$ ) part of the frequency-dependent permittivity of the prepared films was determined using the below relation (1).<sup>70</sup>

$$\epsilon' = \frac{C_p t}{\epsilon_{0A}}, \quad (1)$$

where  $C_p$  is the film capacitance,  $t$  is the film thickness,  $A$  is the surface area of the electrodes, and  $\epsilon_0$  is the permittivity of free space which is  $8.85 \times 10^{-12}$  F/m.

The dielectric investigation of nanopolymer composites is vital because the polymer composites' high dielectric nature allows them to be used in power electronics, printable circuit boards, and miniaturization of electronic equipment.<sup>71</sup> The real part of dielectric constant with varying frequency and various temperatures is shown in Figure 7. The  $\epsilon'$  value of pure PANI film for 100 Hz is 3919. The pure PANI film's  $\epsilon'$  values drop nonlinearly with increasing frequency and it increases with increasing temperature. The PANI film's molecular mobility may increase with temperature, resulting in an improved polarization response and ultimately higher permittivity,<sup>72</sup> and also, the reduction in  $\epsilon'$  values with increasing frequency could be attributed to the contribution of the interfacial polarization (IP) effect, also known as the Maxwell–Wagner–Sillars effect and frequently noted in

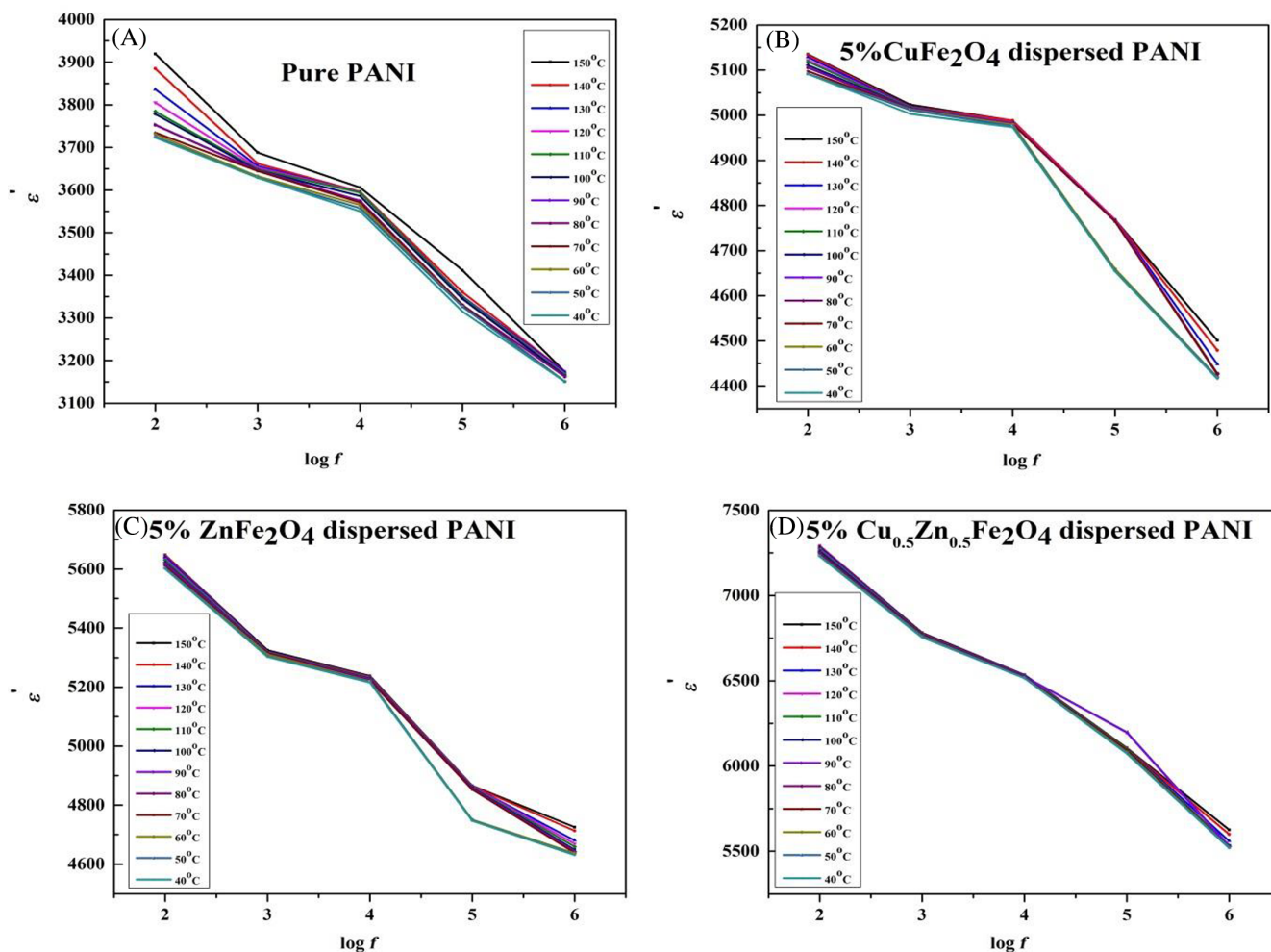


**FIGURE 7** Real part of the dielectric constant with varying log frequency and temperature for the prepared (A) pure polyaniline (PANI), (B) 5 wt.%  $\text{CuFe}_2\text{O}_4$ , (C) 5 wt.%  $\text{ZnFe}_2\text{O}_4$ , and (D) 5 wt.%  $\text{Cu}_{0.5}\text{Zn}_{0.5}\text{Fe}_2\text{O}_4$  dispersed PANI films.

PANI materials.<sup>73</sup> On rare occasions, some literature's make it evident that the  $\epsilon'$  exhibits frequency variation; when the filler content increases to a certain level, the  $\epsilon'$  falls off as the frequency increases. This occurred as a result of the loading being increased further, which caused the permittivity to decrease with the volume percent of filler material. The low-frequency plasma oscillation of free electrons in the continuous conductive distribution is responsible for this.<sup>74-77</sup> The main reason of the highest values of  $\epsilon'$  at low frequencies is the accumulation of charges at the interfaces of different material constituents, which creates micro-capacitance throughout the entire size of the material and contributes to an increase in  $\epsilon'$  at low frequencies. In addition, it is noted that the dielectric constant  $\epsilon'$  rises for the three different inorganic NPs ( $\text{CuFe}_2\text{O}_4$ ,  $\text{ZnFe}_2\text{O}_4$ , and  $\text{Cu}_{0.5}\text{Zn}_{0.5}\text{Fe}_2\text{O}_4$ ) in a polymer matrix, because the relationships between inorganic NPs and the functional polar groups produce a dipole configuration.<sup>78</sup> Notably for 5 wt.%  $\text{Cu}_{0.5}\text{Zn}_{0.5}\text{Fe}_2\text{O}_4$  dispersed film the rate of increase is found to be comparatively high and the value of  $\epsilon'$  for 100 Hz is 7291. This 5 wt.%  $\text{Cu}_{0.5}\text{Zn}_{0.5}\text{Fe}_2\text{O}_4$  shows increased real part of permittivity by 1.85 times than the bare PANI film, which can be explained as follows: because of some space charge accumulating

at the interface, inorganic NP causes the creation of polarization states in the PANI matrix, and due to this polarization,  $\epsilon'$  has a high value. The system's dipoles are unable to quickly realign themselves at increasing high frequency  $\epsilon'$ . These high  $\epsilon'$  values of 5 wt.% ferrite dispersed PANI films over a wide temperature range (up to 150°C) especially  $\text{Cu}_{0.5}\text{Zn}_{0.5}\text{Fe}_2\text{O}_4$  dispersed PANI films.

High dielectric loss can have a significant impact on the real-world application of high dielectric polymer films.<sup>71</sup> Figure 8 shows the change of dielectric loss as a function of frequency for bare and NP dispersed PANI films.

The bare PANI film has dielectric loss nearly 0.09. With the dispersion of 5 wt.% different ferrite NPs, the dielectric loss was decreased by as low as bare film. This dielectric tangent loss is mainly affected by polarization loss and conductivity loss.<sup>79</sup> Notably, PANI polymer films with varying ferrite dispersions all have dielectric loss tangent values  $<0.1$ , which is acceptable for some applications like decoupling capacitors. The superior dispersion of different kinds of ferrite NPs in the polymer matrix is responsible for the minimal dielectric tangent loss. Loss values obtained in our present study for ferrite dispersed PANI films are slightly higher than commercially used



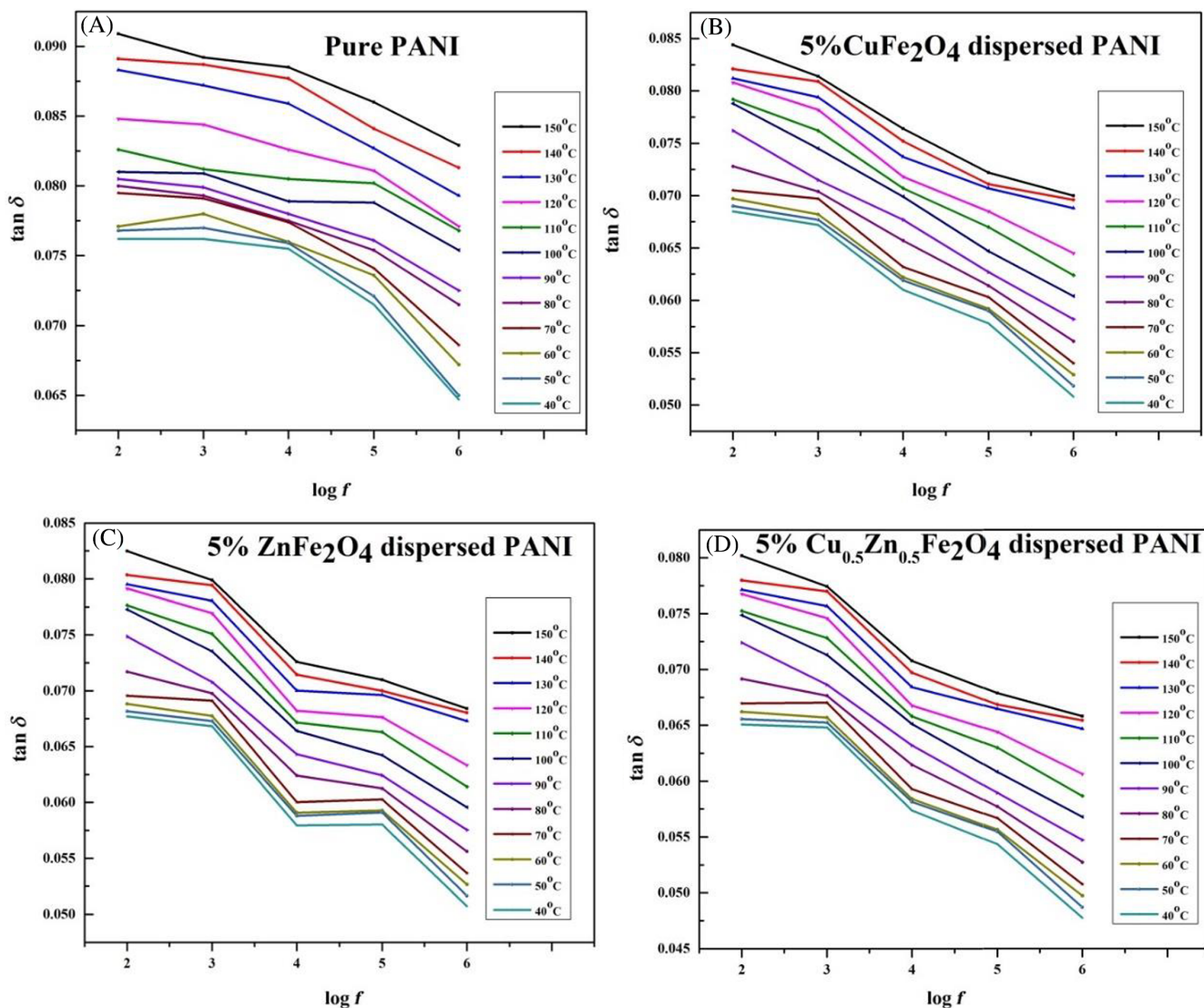


**FIGURE 8** Dielectric loss with varying log frequency and temperature for the prepared (A) pure polyaniline (PANI), (B) 5 wt.%  $\text{CuFe}_2\text{O}_4$ , (C) 5 wt.%  $\text{ZnFe}_2\text{O}_4$ , and (D) 5 wt.%  $\text{Cu}_{0.5}\text{Zn}_{0.5}\text{Fe}_2\text{O}_4$  dispersed PANI films.

polyvinylidene fluoride (PVDF) film whose values are in the range of 0.02–0.05.<sup>80</sup> Quite interesting fact that, to improve dielectric constant and to reduce loss in PVDF, researchers take much effort in controlling their crystalline phase or by controlling their copolymer.<sup>80</sup> However, in our present study, we obtained the prerequisite of modern electronics equipment without any much effort on controlling phases or by controlling concentrations. So, these films are superior to replace PVDF like films in future.<sup>80</sup> High dielectric constant materials can aid in achieving a high Q-factor, which is a measure of a resonator's efficiency. A high-Q resonator can store and release energy with minimum loss, making it appropriate for a wide range of radio frequency and microwave applications. When contrasted with traditional ceramic or metallic resonators, using high-dielectric constant polymers enables for smaller and more compact resonators, which is advantageous for miniaturization and integration in current electronics.

Figure 9 shows that the AC conductivity of bare and 5 wt.% inorganic NP dispersed PANI films which increase with the increase of frequency at several temperatures between 40 and 150°C. The bare PANI film has AC conductivity for 1 MHz at 150°C is  $14,623 \times 10^{-4}$  mho/cm. Furthermore, the AC conductivity may be totally hidden at low modulation frequencies and/or at high measuring temperatures. Higher frequency activity is caused by conductive particles. In terms of dielectric characteristics, this is how semiconductor materials typically behave.<sup>81</sup> The electrical conductivity of functionalized three different ferrite NP dispersed PANI films was increased from  $17,521 \times 10^{-4}$  to  $20,583 \times 10^{-4}$  S/cm, this enhancement was attributed to the charge transfer mechanism. The conductivity of PANI film increased significantly to  $20,583 \times 10^{-4}$  S/cm after 5 wt.%  $\text{Cu}_{0.5}\text{Zn}_{0.5}\text{Fe}_2\text{O}_4$  dispersion, showing the effectiveness of 5 wt.%- $\text{Cu}_{0.5}\text{Zn}_{0.5}\text{Fe}_2\text{O}_4$  NP in improving the conductivity of PANI film. These obtained values for polymer films are notably higher than the

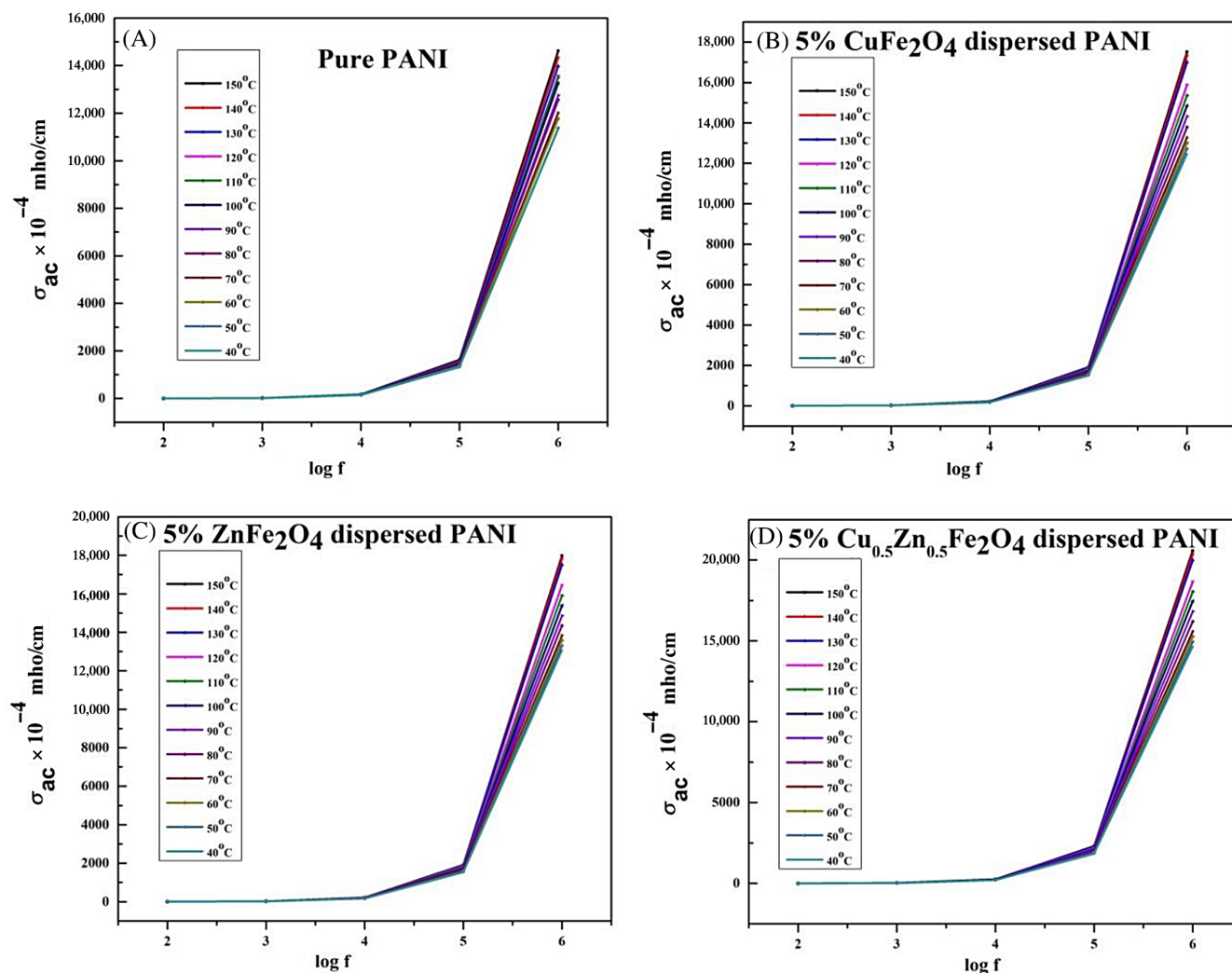


**FIGURE 9** AC conductivity with varying log frequency and temperature for the prepared (A) pure polyaniline (PANI), (B) 5 wt.%  $\text{CuFe}_2\text{O}_4$ , (C) 5 wt.%  $\text{ZnFe}_2\text{O}_4$ , and (D) 5 wt.%  $\text{Cu}_{0.5}\text{Zn}_{0.5}\text{Fe}_2\text{O}_4$  dispersed PANI films.

previously reported conducting polymers.<sup>82,83</sup> Dispersed PANI films exhibit enhanced AC conductivity which in turn shows reduced resistivity in all frequency ranges than the pure PANI films. It was expected that the three different ferrite NPs in this paper would have a beneficial effect on the electrical conductivity of PANI polymer, because the electrical conductivity of three different ferrites dispersed PANI films is much higher than that of the bare PANI film used in this study. A 5 wt.%  $\text{Cu}_{0.5}\text{Zn}_{0.5}\text{Fe}_2\text{O}_4$  NPs have the ability to be valuable conducting filler in polymer composites due to their distinct properties, which other filler materials rarely have. These properties include reduced contact resistance in PANI matrix, high aspect ratios, and increased electrical conductivity that make them ideal for use in electrical devices like sensors and supercapacitor.<sup>84</sup>

### 3.5 | Modulus spectra

IP is almost always present in polymers and hybrid polymeric materials due to the additives, fillers, or even contaminants that make these

systems heterogeneous. IP is usually masked by conductivity in systems with conductive components, and dielectric permittivity can be very high at low frequencies.<sup>85</sup> Although there is continuing questions regarding the utility of the modulus formalism,<sup>86</sup> it has been extensively used to analyze the electrical conductivity data in ionic conductors and polymers to get around this problem.

The complex modulus ( $M^*$ ) can be expressed by the following formulas (2) and (3).<sup>87</sup>

$$M^* = \frac{1}{\epsilon' + i\epsilon''}. \quad (2)$$

$$M^* = M' - iM''. \quad (3)$$

The values of real ( $M'$ ) and imaginary ( $M''$ ) part of the complex modulus can be obtained by the following Relations (4) and (5).<sup>88</sup>

$$M' = \frac{\epsilon'}{(\epsilon'^2 + \epsilon''^2)}. \quad (4)$$

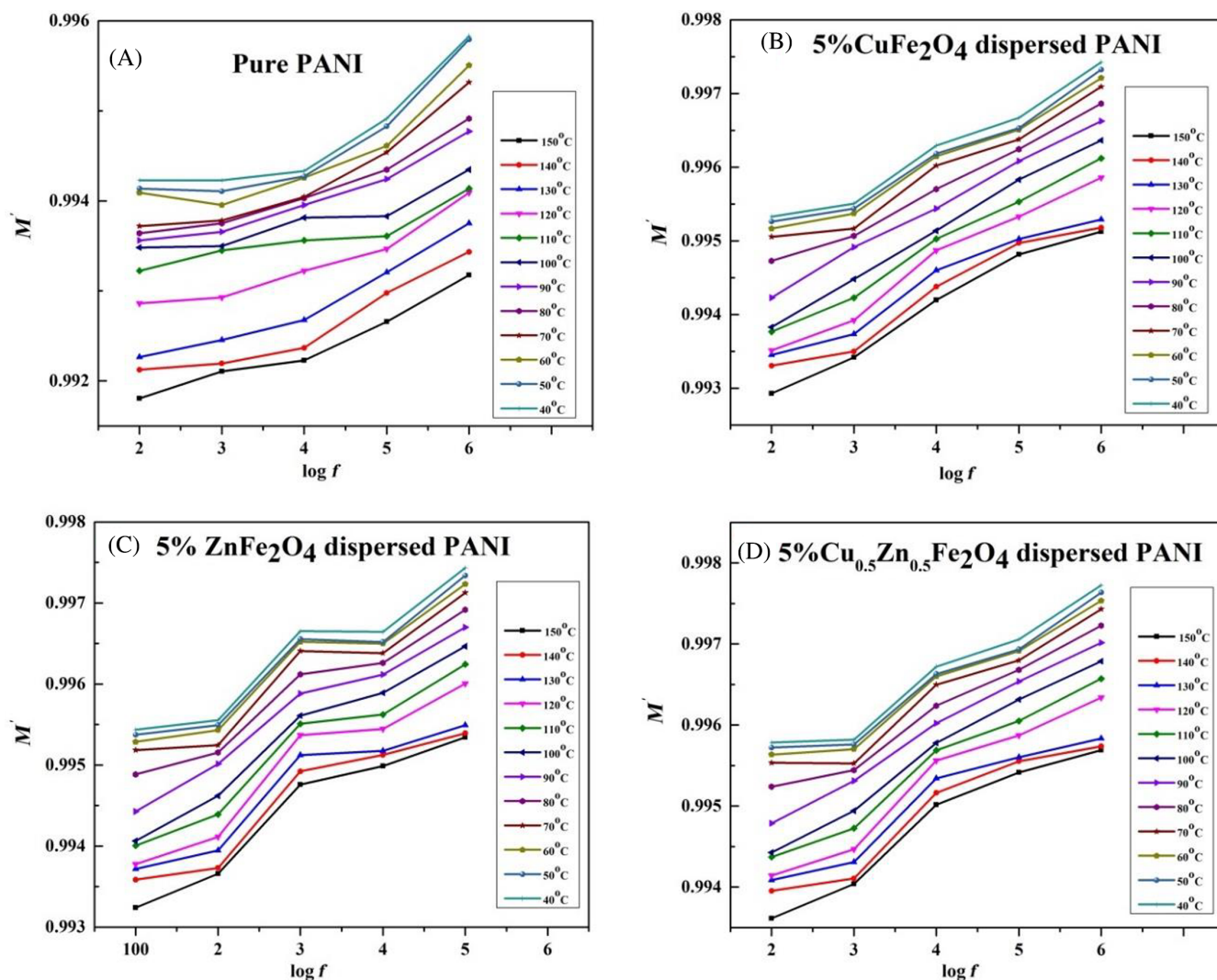


**FIGURE 10** Real modulus part of the modulus spectra with varying log frequency and temperature for the prepared (A) pure polyaniline (PANI), (B) 5 wt.%  $\text{CuFe}_2\text{O}_4$ , (C) 5 wt.%  $\text{ZnFe}_2\text{O}_4$ , and (D) 5 wt.%  $\text{Cu}_{0.5}\text{Zn}_{0.5}\text{Fe}_2\text{O}_4$  dispersed PANI films.

$$M'' = \frac{\epsilon''}{(\epsilon'{}^2 + \epsilon''{}^2)}. \quad (5)$$

Figures 10 and 11 show the spectra of the real  $M'$  and imaginary  $M''$  portions of the electric modulus for pure PANI and 5 wt.% inorganic NP dispersed PANI films at various temperature and frequencies.

The frequency dependence of the  $M'$  values is found to gradually increase as frequency increases throughout the entire frequency range, indicating that there is no electric polarization effect contributing to the noticed  $\epsilon'$  spectra of these materials, because the  $M'$  and  $M''$  values of a composite dielectric material remain close to zero and are also frequency independent over this frequency range.<sup>89</sup> The  $M''$  shows a relaxation peak in the high frequency region that corresponds to the conductivity relaxation process and is mostly found in charge conducting dielectric materials.<sup>90</sup> These high modulus films are recommended for display technology substrates that support essential

components like touch sensor panels, thin film transistors, and the device's viewing screen through cover windows.<sup>91</sup>

## 4 | CONCLUSIONS

Lightweight, cost-effective, and adaptable PANI-ferrite polymer composite films were cast using an environmentally benign and cost-effective approach. Prepared ferrite NP's narrow size distribution, evidence the superiority of solution combustion technique with egg albumen as fuel. Narrow nanosized filler with high surface area of the casted films enhances the dielectric constant and their AC conductivity. Room temperature values of dielectric constant of ferrites dispersed PANI films are noticeably higher in all range of frequency than the commercially available polymer dielectrics. Especially 5 wt.%  $\text{Cu}_{0.5}\text{Zn}_{0.5}\text{Fe}_2\text{O}_4$  dispersed PANI films that exhibit high

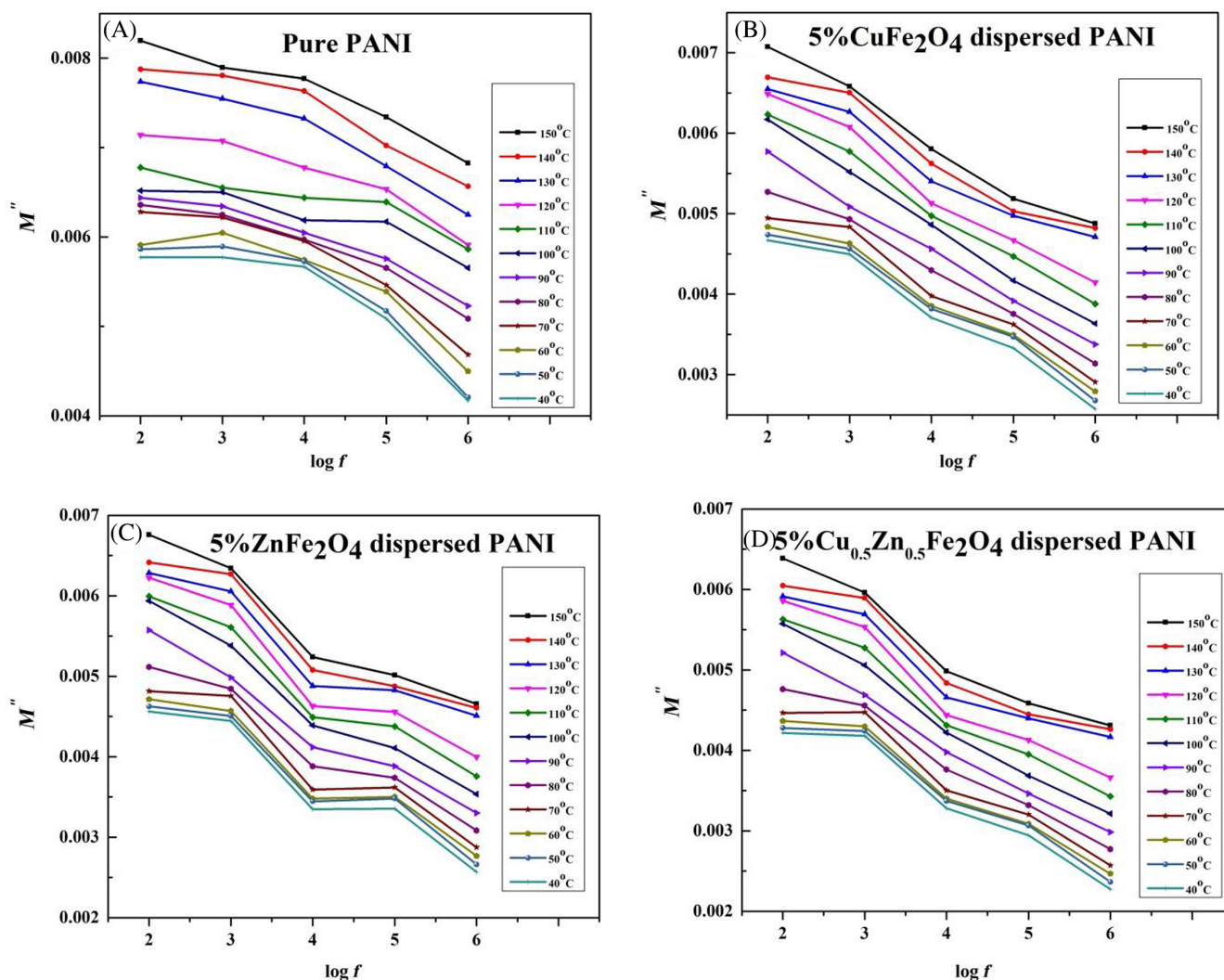


**FIGURE 11** Imaginary modulus part of the modulus spectra with varying log frequency and temperature for the prepared (A) pure polyaniline (PANI), (B) 5 wt.%  $\text{CuFe}_2\text{O}_4$ , (C) 5 wt.%  $\text{ZnFe}_2\text{O}_4$ , and (D) 5 wt.%  $\text{Cu}_{0.5}\text{Zn}_{0.5}\text{Fe}_2\text{O}_4$  dispersed PANI films.

dielectric permittivity with low loss is the solution for the key issue in the flexible dielectrics which can be made by adding high concentration fillers in bare polymer matrix. Thus, the present research is the key solution to the researchers of polymer dielectrics, to process flexible films of high  $\epsilon'$  with ease of fabrication with less concentration of nanofillers.

#### ACKNOWLEDGMENTS

This work is funded by Researcher Supporting Project number RSPD2024R680, King Saud University, Riyadh, Saudi Arabia.

#### DATA AVAILABILITY STATEMENT

Data sharing is not applicable to this article as no new data were created or analyzed in this study.

#### ORCID

Tamilarasi Kumar <https://orcid.org/0000-0003-2238-7923>

Aji Udhaya Paul Raj <https://orcid.org/0000-0002-1689-0007>

Meena Muthukrishnan <https://orcid.org/0000-0002-0970-7761>

Senthil Muthu Kumar Thiagamani <https://orcid.org/0000-0003-1443-7222>

Shaikh Ayaz Mukarram <https://orcid.org/0000-0002-0410-5286>

#### REFERENCES

- Wang P, Song T, Abo-Dief HM, et al. Effect of carbon nanotubes on the interface evolution and dielectric properties of polylactic acid/ethylene-vinyl acetate copolymer nanocomposites. *Adv Compos Hybrid Mater.* 2022;5:1100-1110. doi:10.1007/s42114-022-00489-0
- Wang Y, Yang D, Hessian MM, et al. Flexible barium titanate@polydopamine/polyvinylidene fluoride/polymethyl methacrylate nanocomposite films with high performance energy storage. *Adv Compos Hybrid Mater.* 2022;5:2106-2115. doi:10.1007/s42114-022-00552-w
- Ma R, Cui B, Hu D, et al. Enhanced energy storage of lead-free mixed oxide core double-shell barium strontium zirconatetitanate @ magnesium aluminate @ zinc oxide-boron trioxide-silica ceramic nanocomposites. *Adv Compos Hybrid Mater.* 2022;5:1477-1489. doi:10.1007/s42114-022-00509-z
- Zijian W, Wang X, Annamareddy SHK, et al. Dielectric properties and thermal conductivity of polyvinylidene fluoride synergistically

- enhanced with silica @ multi-walled carbon nanotubes and boron nitride. *ES Mater Manuf.* 2023;22:847. doi:10.30919/esmm5f847
5. He R, Nantung T, Olek J, Na L. Use of dielectric constant for determination of water-to-cement ratio (W/C) in plastic concrete: part 1 volumetric water content modeling. *ES Mater Manuf.* 2023;21:866. doi:10.30919/esmm5f866
  6. Dang ZM, Yuan JK, Yao SH, Liao RJ. Flexible nanodielectric materials with high permittivity for power energy storage. *Adv Mater.* 2013;25:6334-6365.
  7. Chu BJ, Zhou X, Ren KL, et al. A dielectric polymer with high electric energy density and fast discharge speed. *Science.* 2006;313:334-336.
  8. Roy HS, Mominul Islam M Yousuf A., Mollah M, Abu Bin Hasan Susan M. Polyaniline-NiO nanocomposites as dielectric materials. *Mater Today: Proc.* 2018;5:15267-15276. doi:10.1016/j.matpr.2018.05.005
  9. Nalwa H. *Handbook of Low and High Dielectric Constant Materials and Their Applications.* Phenomena, Properties and Applications. Vol 2. Academic Press; 1999.
  10. Kakade AB, Deshpande SK, Kulkarni SB. Electrical conductivity and modulus studies of  $x$  [CNFO]- $(1-x)$  [0.5BCT-0.5BZT] multiferroic with dielectric magnetic and magneto-dielectric properties. *Eng Sci.* 2022;18:168-176. doi:10.30919/es8d485
  11. Antonel P, Berho FM, Jorge G, Molina FV. Magnetic composites of CoFe<sub>2</sub>O<sub>4</sub> nanoparticles in a poly (aniline) matrix: enhancement of remanence ratio and coercivity. *Synth Met.* 2015;199:292e302.
  12. Hashim M, Alimuddin SE, Shirsath SS, et al. Study of structural and magnetic properties of (Co-Cu)Fe<sub>2</sub>O<sub>4</sub>/PANI composites. *Mater Chem Phys.* 2013;141:406e415.
  13. Apesteguy JC, Jacobo SE. Composite of polyaniline containing iron oxides. *Physica B.* 2004;354(1-4):224-227.
  14. Stejskal J, Trchova M, Brodinova J, et al. Coating of zinc ferrite particles with a conducting polymer, polyaniline. *J Colloid Interface Sci.* 2006;298:87-93.
  15. Mouallem Bahout M, Bertrand S, Pena O. Synthesis and characterization of Zn<sub>1-x</sub>Ni<sub>x</sub>Fe<sub>2</sub>O<sub>4</sub> spinels prepared by a citrate precursor. *J Solid State Chem.* 2006;178(4):1080-1086.
  16. Yahya N, Aripin A, Aziz A, et al. Synthesis and characterization of magnesium zinc ferrites as electromagnetic source. *Am J Eng Appl Sci.* 2008;1(1):53-56.
  17. Ming M, Zhang Y, Xiaobo L, Degang F, Haiqian Z, Ning G. Synthesis and characterization of titania coated Mn-Zn ferrite nanoparticles. *Colloids Surf A: Physicochem Eng Asp.* 2003;224(1-3):207-212.
  18. Kenfack F, Langben H. Influence of the starting powders on the synthesis of nickel ferrite. *Cryst Res Technol.* 2006;41(8):748-758.
  19. Yao L, Zhao J, Jaecai H. Self-propagating high temperature synthesis and magnetic properties of Ni<sub>0.35</sub>Zn<sub>0.65</sub>Fe<sub>2</sub>O<sub>4</sub> powders. *Bull Mater Sci.* 2002;25(4):263-266.
  20. Khanvilkar MB, Nikumbh AK, Pawar RA, et al. Effect of divalent/trivalent doping on structural, electrical and magnetic properties of spinel ferrite nanoparticles. *Eng Sci.* 2023;22:850. doi:10.30919/es8d850
  21. Rasheed TA, Afotey B, Ankudey EG, Anang DA. Synthesis and characterization of novel calcium oxide/calcium ferrite, CaO/CaFe<sub>2</sub>O<sub>4</sub> composite nano catalyst for biodiesel production. *ES Mater Manuf.* 2023;22:922. doi:10.30919/esmm922
  22. Ji L, Shen X, Zhao R, et al. Isotropic ferromagnetic resonances induced by suppressed anisotropy in soft magnetic microstructures. *Eng Sci.* 2022;19:136-143. doi:10.30919/es8d711
  23. Yao H, Wang S, Lei M, Bi K. Magnetically tunable wideband ferrite-based metamaterial phase shifter. *Eng Sci.* 2021;16:301-307. doi:10.30919/es8d549
  24. Verma A, Saxena AK, Dube DC. Microwave permittivity and permeability of ferrite-polymer thick films. *J Magn Magn Mater.* 2003;263:228-234. doi:10.1016/S0304-8853(02)01569-X
  25. Hussain HV, Ahmad M, Ansar MT, et al. Polymer based nickel ferrite as dielectric composite for energy storage applications. *Synth Met.* 2020;268:116507. doi:10.1016/j.synthmet.2020.116507
  26. Chen W-C, Wen T-C. Electrochemical and capacitive properties of polyaniline-implanted porous carbon electrode for supercapacitors. *J Power Sources.* 2003;117:273-282. doi:10.1016/S0378-7753(03)00158-7
  27. Taleghani HG, Aleahmad M, Eisazadeh H. Optical properties of prepared polyaniline and polymethylmethacrylate blends. *World Appl Sci J.* 2009;6(12):1607-1611.
  28. Song E, Choi JW. Conducting polyaniline nanowire and its applications in chemiresistive sensing. *Nanomaterials (Basel).* 2013;3(3):498-523. doi:10.3390/nano3030498
  29. Reda S, Al-Ghannam SM. Synthesis and electrical properties of polyaniline composite with silver nanoparticles. *Adv Mater Phys Chem.* 2012;2:75-81.
  30. Vyas S, Shukla A, Shivhare SJ, Bagal VS, Upadhyay N. High performance conducting nanocomposites polyaniline (PANI)-CuO with enhanced antimicrobial activity for biomedical applications. *ES Mater Manuf.* 2022;15:46-52. doi:10.30919/esmm5f468
  31. Liao Y, Wang Y, Ouyang LF, et al. Conductive polyaniline enhanced decolorization of azo dyes in anaerobic wastewater treatment. *ES Food Agrofor.* 2021;6:35-42. doi:10.30919/esfaf584
  32. Junyan L, Yang Y, Zhong Y, Qian H, Qiu B. The study on activated carbon, magnetite, polyaniline and polypyrrole development of methane production improvement from wastewater treatment. *ES Food Agrofor.* 2022;10:30-38. doi:10.30919/esfaf802
  33. Lan D, Wang Y, Wang Y, et al. Impact mechanisms of aggregation state regulation strategies on the microwave absorption properties of flexible polyaniline. *J Colloid Interface Sci.* 2023;651:494-503. doi:10.1016/j.jcis.2023.08.019
  34. Fonseca SGC, Neivab LS, Bonifácio MAR, et al. Tunable magnetic and electrical properties of cobalt and zinc ferrites CO<sub>1-x</sub>Zn<sub>x</sub>Fe<sub>2</sub>O<sub>4</sub> synthesized by combustion route. *Mater Res.* 2018;21(3):e20170861. doi:10.1590/1980-5373-MR-2017-0861
  35. Kazantseva N, Vilčáková J, Křesálek V, Saha P, Sapurina I, Stejskal J. Magnetic behaviour of composites containing polyaniline-coated manganese-zinc ferrite. *J Magn Magn Mater.* 2004;269:30-37. doi:10.1016/S0304-8853(03)00557-2
  36. Khairy M. Polyaniline-Zn<sub>0.2</sub>Mn<sub>0.8</sub>Fe<sub>2</sub>O<sub>4</sub> ferrite core-shell composite: preparation, characterization and properties. *J Alloys Compds.* 2014;608:283e291.
  37. Chitra P, Muthusamy A, Dineshkumar S, Prakash R, Chandrasekar J. Temperature and frequency dependence on electrical properties of polyaniline/Ni<sub>(1-x)</sub>CoxFe<sub>2</sub>O<sub>4</sub> nanocomposites. *J Magn Magn Mater.* 2015;384:204e212.
  38. Gabal MA, Al-Juaid AA, El-Rashed S, Hussein MA, Al Angari YM. Polyaniline/Co<sub>0.6</sub>Zn<sub>0.4</sub>Fe<sub>2</sub>O<sub>4</sub> core-shell nano-composites. Synthesis, characterization and properties. *J Alloys Compds.* 2018;747:83-90.
  39. Tamilarasi K, AjiUdhaya P, Meena M. Enhancement on the electrical and optical behaviour of ZnFe<sub>2</sub>O<sub>4</sub> nano particles via transition metal substitution. *Mater Today Proc.* 2022;64:1671-1678. doi:10.1016/j.matpr.2022.05.35
  40. Ilyas RA, Sapuan SM, Kadier A, et al. Properties and characterization of PLA, PHA, and other types of biopolymer composites. *Advanced Processing, Properties, and Applications of Starch and Other Bio-Based Polymers.* Elsevier; 2020:111-138. doi:10.1016/b978-0-12-819661-8.00008-1
  41. Sari NH, Suteja S, Fudholi A, et al. Morphology and mechanical properties of coconut shell powder-filled untreated cornhusk fibre-unsaturated polyester composites. *Polymer.* 2021;222:123657. doi:10.1016/j.polymer.2021.123657
  42. Sari NH, Setyawan PD, Thiagamani SMK, Suteja RT, Rangappa SM, Siengchin S. Evaluation of mechanical, thermal and morphological properties of corn husk modified pumice powder reinforced polyester

- composites. *Polym Compos.* 2022;43:1763-1771. doi:[10.1002/pc.26495](https://doi.org/10.1002/pc.26495)
43. Sari NH, Suteja S, Fudholi A, et al. Evaluation of impact, thermo-physical properties, and morphology of cornhusk fiber-reinforced polyester composites. *Polym Compos.* 2022;43:2771-2778. doi:[10.1002/pc.26573](https://doi.org/10.1002/pc.26573)
  44. Beygisangchin M, Abdul Rashid S, Shafie S, Sadrolhosseini AR, Lim HN. Preparations, properties, and applications of polyaniline and polyaniline thin films-a review. *Polymers (Basel).* 2021;13(12):2003. doi:[10.3390/polym13122003](https://doi.org/10.3390/polym13122003)
  45. Ajeel KI, Kareem QS. Synthesis and characteristics of polyaniline (PANI) filled by graphene (PANI/GR) nano-films. *J Phys: Conf Ser.* 2019;1234:012020. doi:[10.1088/1742-6596/1234/1/012020](https://doi.org/10.1088/1742-6596/1234/1/012020)
  46. Hwang J, Choi M, Shin H-S, Ju B-K, Chun M. Structural and magnetic properties of NiZn ferrite nanoparticles synthesized by a thermal decomposition method. *Appl Sci.* 2020;10:6279. doi:[10.3390/app10186279](https://doi.org/10.3390/app10186279)
  47. Abo AT, Altimari P, Moscardini E, Pettiti I, Toro L, Pagnanelli F. Synthesis and characterization of copper ferrite magnetic nanoparticles by hydrothermal route. *Chem Eng Trans.* 2016;47:151-156. doi:[10.3303/CET1647026](https://doi.org/10.3303/CET1647026)
  48. Borade RM, Somvanshi SB, Kale SB, Pawar RP, Jadhav KM. Spinel zinc ferrite nanoparticles: an active nanocatalyst for microwave irradiated solvent free synthesis of chalcones. *Mater Res Express.* 2020;7:016116. doi:[10.1088/2053-1591/ab6c9c](https://doi.org/10.1088/2053-1591/ab6c9c)
  49. Padmapriya S, Harinipriya S, Jaidev K, Sudha V, Kumar D, Pal S. Storage and evolution of hydrogen in acidic medium by polyaniline. *Int J Energy Res.* 2017;42:1196-1209. doi:[10.1002/er.3920](https://doi.org/10.1002/er.3920)
  50. Sengupta PP, Barik S, Adhikari B. Polyaniline as a gas-sensor material. *Mater Manuf Process.* 2006;21:263-270. doi:[10.1080/10426910500464602](https://doi.org/10.1080/10426910500464602)
  51. Wei Y, Sun Y, Jang GW, Tang X. Effects of p-aminodiphenylamine on electrochemical polymerization of aniline. *J Polym Sci Part C: Polym Lett.* 1990;28(3):81-87.
  52. Jiji A, Joseph N, Donald RB, Daniel M, Amit S, Qiang Y. Size-dependent specific surface area of nanoporous film assembled by core-shell iron nanoclusters. *J Nanomater.* 2006;2006:54961. doi:[10.1155/JNM/2006/54961](https://doi.org/10.1155/JNM/2006/54961)
  53. Zhang J, Xiao X, Nan J. Hydrothermal-hydrolysis synthesis and photocatalytic properties of nano TiO<sub>2</sub> with an adjustable crystalline size. *J Hazard Mater.* 2010;176:617-622.
  54. Aghazadeh M, Aghazadeh F. Green chemistry method with XRD analyzes and absorption of TiO<sub>2</sub> nanoparticles modified with use of choline chloride. *Int J Bio-Inorg Hybrid Nanomater.* 2018;7(2):97-108.
  55. Shen Y, Yamazaki T, Liu Z, Meng D, Kikuta T, Nakatani N. Influence of effective surface area on gas sensing properties of WO<sub>3</sub> sputtered thin films. *Thin Solid Films.* 2009;517:2069-2072. doi:[10.1016/j.tsf.2008.10.021](https://doi.org/10.1016/j.tsf.2008.10.021)
  56. Gomez-Pozos H, González-Vidal JL, Torres GA, OlveraMde L, Castaneda L. Physical characterization and effect of effective surface area on the sensing properties of tin dioxide thin solid films in a propane atmosphere. *Sensors (Basel).* 2013;14:403-415. doi:[10.3390/s140100403](https://doi.org/10.3390/s140100403)
  57. Biasotto G, Ranieri MGA, Foschini C, Simões AZ, Longo E, Zaghete MA. Gas sensor applications of zinc oxide thin film grown by the polymeric precursor method. *Ceram Int.* 2014;40:14991-14996. doi:[10.1016/j.ceramint.2014.06.099](https://doi.org/10.1016/j.ceramint.2014.06.099)
  58. Nagendra B, Cozzolino A, Daniel C, Rizzo P, Guerra G. High surface area nanoporous-crystalline polymer films. *Macromolecules.* 2022;55:2983-2990. doi:[10.1021/acs.macromol.2c00271](https://doi.org/10.1021/acs.macromol.2c00271)
  59. Bhadra S, Chattopadhyay S, Singha NK, Khastgir D. Improvement of conductivity of electrochemically synthesized polyaniline. *J Appl Polym Sci.* 2008;108:57-64.
  60. Shaban M, Abukhadra MR, Rabia M, Elkader YA, El-Halim A, Mai R. Investigation the adsorption properties of graphene oxide and polyanilinenano/micro structures for efficient removal of toxic Cr (VI) contaminants from aqueous solutions; kinetic and equilibrium studies. *Rend Lincei Sci Fis E Nat.* 2018;29:141-154.
  61. Shao W, Jamal R, Feng X, Ubul A, Abdiryim T. The effect of a small amount of water on the structure and electrochemical properties of solid-state synthesized polyaniline. *Materials.* 2012;5:1811-1825. doi:[10.3390/ma5101811](https://doi.org/10.3390/ma5101811)
  62. Kellenberger A, Dmitrieva E, Dunsch L. Structure dependence of charged states in "linear" polyaniline as studied by in situ ATR-FTIR Spectro electrochemistry. *J Phys Chem B.* 2012;116(14):4377-4385.
  63. Nyffenegger R, Gerber C, Siegenthaler H. In situ investigation of electropolymerized polyaniline films by scanning tunneling microscopy. *Synth Met.* 1993;55:402-407. doi:[10.1016/0379-6779\(93\)90965-Y](https://doi.org/10.1016/0379-6779(93)90965-Y)
  64. Duic LJ, Mandic Z, Kovacicek F. The effect of supporting electrolyte on the electrochemical synthesis, morphology, and conductivity of polyaniline. *J Polym Sci A Polym Chem.* 1994;32(1):105-111. doi:[10.1002/pola.1994.080320112](https://doi.org/10.1002/pola.1994.080320112)
  65. Ajmal M, Islam MU. Structural, optical and dielectric properties of polyaniline-Ni<sub>0.5</sub>Zn<sub>0.5</sub>Fe<sub>2</sub>O<sub>4</sub> nano-composites. *Physica B: Condens Matter.* 2017;521:355-360. doi:[10.1016/j.physb.2017.07.010](https://doi.org/10.1016/j.physb.2017.07.010)
  66. Kumar KK, Sathaiah G, Sirdeshmukh L. Dielectric properties and electrical conductivity studies on Gd<sub>3</sub>Ga<sub>5</sub>O<sub>12</sub> single crystals. *Int J Chem Sci.* 2011;9(1):239-244.
  67. Meena M, Mahadevan CK, Sakthisundarasaravanan R, Praveen VN. Effect of added impurities on the properties of LAHCL single crystals. *Int J Macro Nano Phys.* 2016;1(1):12-18.
  68. Meena M, Mahadevan CK. Growth and dielectric properties of L-arginine acetate and L-arginine oxalate single crystals. *Mater Lett.* 2008;62(21-22):3742-3744.
  69. Suganya K, Maalmarugan J, Manikandan R, et al. Synthesis, studies of 2-benzyl-amino-4-p-tolyl-6,7-di-hydro 5H-cyclo-penta-[b]pyridine-3 carbo-nitrile (BAPTDHPCPN) crystals for optical, photonic and mechano-electronic uses. *J Mater Sci Mater Electron.* 2022;33:19320-19330. doi:[10.1007/s10854-022-08770-0](https://doi.org/10.1007/s10854-022-08770-0)
  70. Sindhu S, Anantharaman MR, Thampi BP, Malini KA, Kurian P. Evaluation of a.c. conductivity of rubber ferrite composites from dielectric measurements. *Bull Mater Sci.* 2002;25:599-607. doi:[10.1007/BF02707892](https://doi.org/10.1007/BF02707892)
  71. El-Bashir SM, Alwadai NM, AlZayed N. AC/DC electrical conduction and dielectric properties of PMMA/PVAc/C60 down-shifting nanocomposite films. *J Mol Struct.* 2018;1154:239-247.
  72. Das M, Akbar A, Sarkar D. Investigation on dielectric properties of polyaniline (PANI) sulphonic acid (SA) composites prepared by interfacial polymerization. *Synth Met.* 2019;249:69-80. doi:[10.1016/j.synthmet.2019.02.004](https://doi.org/10.1016/j.synthmet.2019.02.004)
  73. Choudhary S. Structural and dielectric properties of (PEO-PMMA)-SnO<sub>2</sub> nanocomposites. *Compos Commun.* 2017;5:54-63. doi:[10.1016/j.coco.2017.07.004](https://doi.org/10.1016/j.coco.2017.07.004)
  74. Wei Z, Zhang G, Song X, et al. State and negative permittivity in LaCo<sub>1-x</sub>Ni<sub>x</sub>O<sub>3</sub> ceramics. *Eng Sci.* 2023;21:806. doi:[10.30919/es8d806](https://doi.org/10.30919/es8d806)
  75. Li X, Meng S, Xie P, et al. Two percolation behaviors in binary heterogeneous composites for high permittivity and negative permittivity. *Eng Sci.* 2023;21:795. doi:[10.30919/es8d795](https://doi.org/10.30919/es8d795)
  76. Tang X, Zhang Z, Kuma DJP, et al. Flexible carbon nanotubes/polystyrene membranous composites toward ultraweakly and frequency-stable negative permittivity at kHz region. *Eng Sci.* 2023;24:920. doi:[10.30919/es920](https://doi.org/10.30919/es920)
  77. He R, Nantung T, Olek J, Na L. Use of dielectric constant for determination of water-to-cement ratio (W/C) in plastic concrete: part 2 comparison determined W/C values by ground penetrating radar (GPR) and microwave oven drying measurements. *ES Mater Manuf.* 2023; 22:874. doi:[10.30919/esmm5f874](https://doi.org/10.30919/esmm5f874)
  78. Sugumaran S, Bellan CS, Muthu D, Raja S, Bheeman D, Rajamani R. Characterization of composite PVA-Al<sub>2</sub>O<sub>3</sub> thin films prepared by dip coating method. *Iran Polym J.* 2015;24:63-74.

79. Wang Q, Che J, Wu W, et al. Contributing factors of dielectric properties for polymer matrix composites. *Polymers*. 2023;15:590. doi:10.3390/polym15030590
80. Zha J-W, Zheng M-S, Fan B, Dang Z-M. Polymer-based dielectrics with high permittivity for electric energy storage: a review. *Nano Energy*. 2021;89:106438. doi:10.1016/j.nanoen.2021.106438
81. Meena M, Mahadevan CK. Growth and electrical characterization of L-arginine added KDP and ADP single crystals, crystal. *Res Technol*. 2007;43(2):166-172.
82. Husain DJ, Anjum DR, Reddy DN, Sagar J, Anjum B. AC conductivity studies on polyaniline/cobalt oxide nanocomposites thin films. *International Research Journal on Advanced Science Hub (IRJASH)*. 2020;02:41-43.
83. Chauhan SM, Mahida J, Chakrabarty BS. Dielectric property and conductivity study of polyaniline - CaF<sub>2</sub> nanocomposites. *J Nano Adv Mat*. 2016;4(1):9-17. doi:10.18576/jnam/040102
84. Hoppe B, Hindricks KDJ, Warwas DP. Graphene-like metal-organic frameworks: morphology control, optimization of thin film electrical conductivity and fast sensing applications. *CrstEngComm*. 2018;20:6458-6471.
85. Kyrirtsis A, Pissi P, Grammatikakis I. Dielectric relaxation spectroscopy in poly (hydroxyethyl acrylates)/water hydrogels. *J Polym Sci B*. 1995;33:1737-1750.
86. Neagu RM, Neagu N, Bonanes N, Pissis P. Electrical conductivity studies in nylon 11. *J Appl Phys*. 2000;88:6669-6677. doi:10.1063/1.1323752
87. Langar A, Sdiri N, Elhouichet H, Ferid M. Structure and electrical characterization of ZnO-Ag phosphate glasses. *Results Phys*. 2017;7:1022-1029.
88. Tripathi SK, Gupta A, Kumari M. Studies on electrical conductivity and dielectric behaviour of PVdF-HFP-PMMA-NaI polymer blend electrolyte. *Bull Mater Sci*. 2013;35(6):969-975.
89. Bouaamlat H, Hadi N, Belghiti N, et al. Dielectric properties, AC conductivity, and electric modulus analysis of bulk ethylcarbazole-terphenyl. *Adv Mater Sci Eng*. 2020;2020:8689150. doi:10.1155/2020/8689150
90. Dutta A, Sinha TP, Jena P, Adak S. Ac conductivity and dielectric relaxation in ionically conducting soda-ime-silicate glasses. *J Non Cryst Solids*. 2008;354:3952-3957.
91. Wang L, Yu X, Wang D, et al. High modulus and high strength ultra-thin polyimide films with hot-stretch induced molecular orientation. *Mater Chem Phys*. 2013;139:968-974.

**How to cite this article:** Kumar T, Paul Raj AU, Muthukrishnan M, Thiagamani SMK, Hashem M, Mukarram SA. PANI/Zn-Cu ferrite polymer composites as free-standing high dielectric materials. *Polym Adv Technol*. 2024;35(1):e6285. doi:10.1002/pat.6285.